

Ultrathin, Core–Shell Structured SiO₂ Coated Mn²⁺-Doped Perovskite Quantum Dots for Bright White Light-Emitting Diodes

Xiaosheng Tang, Weiwei Chen, Zhengzheng Liu, Juan Du,* Zhiqiang Yao, Yi Huang, Cheng Chen, Zhaoqi Yang, Tongchao Shi, Wei Hu, Zhigang Zang, Yu Chen,* and Yuxin Leng*

All-inorganic semiconductor perovskite quantum dots (QDs) with outstanding optoelectronic properties have already been extensively investigated and implemented in various applications. However, great challenges exist for the fabrication of nanodevices including toxicity, fast anion-exchange reactions, and unsatisfactory stability. Here, the ultrathin, core–shell structured SiO₂ coated Mn²⁺ doped CsPbX₃ (X = Br, Cl) QDs are prepared via one facile reverse microemulsion method at room temperature. By incorporation of a multibranching capping ligand of trioctylphosphine oxide, it is found that the breakage of the CsPbMnX₃ core QDs contributed from the hydrolysis of silane could be effectively blocked. The thickness of silica shell can be well-controlled within 2 nm, which gives the CsPbMnX₃@SiO₂ QDs a high quantum yield of 50.5% and improves thermostability and water resistance. Moreover, the mixture of CsPbBr₃ QDs with green emission and CsPbMnX₃@SiO₂ QDs with yellow emission presents no ion exchange effect and provides white light emission. As a result, a white light-emitting diode (LED) is successfully prepared by the combination of a blue on-chip LED device and the above perovskite mixture. The as-prepared white LED displays a high luminous efficiency of 68.4 lm W⁻¹ and a high color-rendering index of Ra = 91, demonstrating their broad future applications in solid-state lighting fields.

1. Introduction

White light-emitting diodes (LEDs) exhibit long operational lifetime, fast response time, and remarkable energy conservation efficiency, which have received substantial applications in current solid-state lighting and display.^[1–3] The typical white LEDs are mainly made of a blue-emitting InGaN or GaN chip and Ce-doped yttrium aluminum garnet phosphor, which can efficiently convert the blue emission to a quite broad yellow emission.^[4,5] Finally, white light is formed by combining the blue and yellow lights. However, most of the white light achieved by this color-conversion strategy lacks of red and green components in the emission spectrum, which results in low color rendering index (CRI < 80), limited luminous efficiency, as well as high correlated color temperature (CCT) and hampers our pursuit of light quality.^[6,7] Fortunately, alternative quantum dots (QDs) material shares a common feature of narrow and finely

Prof. X. Tang, W. Chen, Dr. W. Hu, Prof. Z. Zang
Key Laboratory of Optoelectronic Technology & Systems
(Ministry of Education)
College of Optoelectronic Engineering
Chongqing University
Chongqing 400044, China

Z. Liu, Prof. J. Du, T. Shi, Prof. Y. Leng
Center of Materials Science and Optoelectronics Engineering
University of Chinese Academy of Sciences
Beijing 100049, China
E-mail: dujuan@mail.siom.ac.cn; lengyuxin@mail.siom.ac.cn

Prof. Z. Yao
State Centre for International Cooperation on Designer Low-Carbon
and Environmental Materials (ICDLCEM)
School of Materials Science and Engineering
Zhengzhou University
Zhengzhou 450001, China

 The ORCID identification number(s) for the author(s) of this article can be found under <https://doi.org/10.1002/sml.201900484>.

Prof. Y. Huang
College of Optoelectronic Engineering
Chongqing University of Posts and Telecommunications
Chongqing 400065, P. R. China

Prof. C. Chen
State Key Laboratory of Advanced Technology
for Materials Synthesis and Processing
School of Materials Science and Engineering
Wuhan University of Technology
Wuhan 430070, China

Prof. Z. Yang
School of Pharmaceutical Sciences
Jiangnan University
Jiangsu 214122, China

Prof. Y. Chen
School of Optoelectronic Science and Engineering & Collaborative
Innovation Center of Suzhou Nano Science and Technology
Soochow University
Suzhou 215006, China
E-mail: chen_yu_ny@suda.edu.cn

DOI: 10.1002/sml.201900484

tunable emission band, making them one suitable candidate in the fabrication of white LEDs with satisfactory luminous quality.

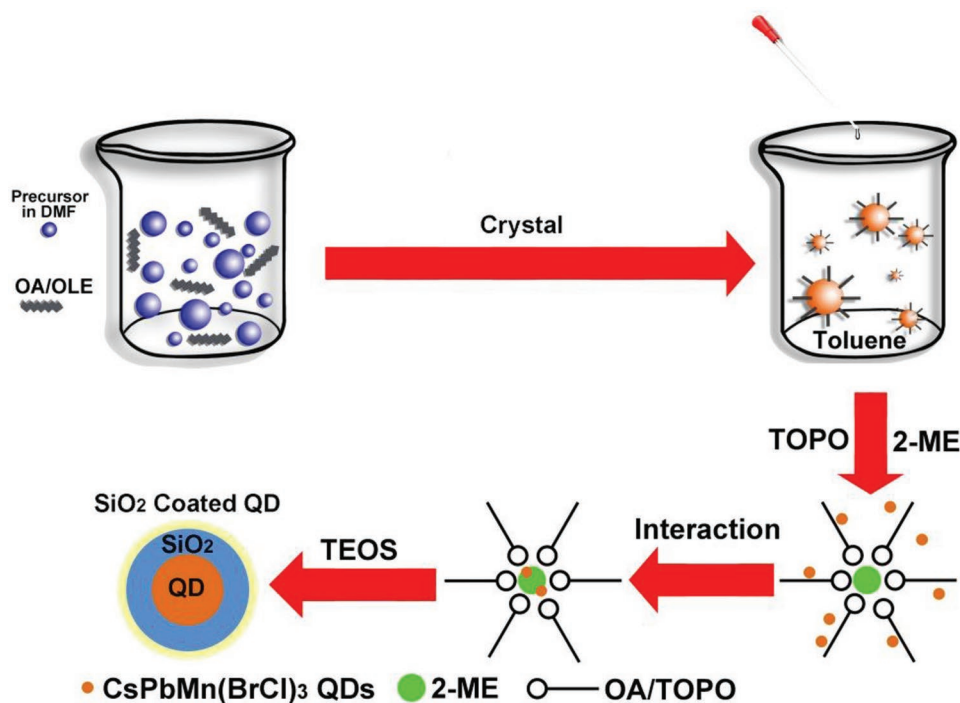
As an attractive optoelectronic material, all-inorganic semiconductor perovskite CsPbX₃ (X = Cl, Br, I) material has aroused extensive interest in the applications of solar cells, lasing, photo-detector, and LEDs owing to their high absorbance coefficient, tunable photoluminescence (PL) spectrum, as well as high PL quantum yield (PLQY) and solution processing capabilities.^[8–13] However, this perovskite material contains an environment unfriendly element of Pb and displays low stability of crystalline structure. This phenomenon results from the strong ionic crystal feature of perovskite material itself in nature, which seriously restricts their further commercial application.^[14–16] To reduce the toxicity of perovskite QDs, great numbers of efforts have been devoted to reduce or substitute lead with nontoxic elements (Ge, Sb, Bi, Sn).^[17] Nevertheless, for the majority of the lead-free perovskite QDs, they often have limitations of low PLQY and poor stability to be applied to regular solid-state lighting, especially under the circumstance of high humidity, high temperature, or irradiation. For example, the reported CsSnX₃ QDs exhibited a maximal PLQY of only 0.14% and could only keep for several hours.^[18] Additionally, nearly all the perovskite QDs have serious self-absorption problem resulting from the small Stokes shift. Therefore, by introducing transition metal ions, e.g., Mn²⁺, into semiconductor QDs to generate new optical and electronic properties to the host QDs, such as large Stoke shifts, high excited state lifetime and environmental stability have been broadly explored.^[19,20] Recently, through the control of the CsPbCl₃ QDs bandgap around 3.1 eV, Dong's group demonstrated that the Mn²⁺ doped CsPbCl₃ QDs exhibit two PL emission peaks located at 410 and 600 nm and one absorption peak around 400 nm.^[21] Moreover, the reduced lead element in the doped perovskite QDs makes them more environmental friendly. Thus, the Mn²⁺ doped perovskite QDs can be identified as one of the promising down conversion phosphors for white LEDs. However, serious ion-exchange effect will occur when these perovskite materials with different composition are directly mixed in solution or in the solid state.^[22,23] Therefore, it is highly desired to seek an effective strategy for enhancing the stability and preventing ion exchange simultaneously for perovskite QDs, which could solve the crucial problems for their application in white LEDs.

Recent researches concentrate on establishing a variety of materials with coating technology to improve the stability of perovskite QDs against the UV-light and moisture.^[24–28] For example, Alivisatos's group integrated the polymer matrices into the synthesis of the colloidal CsPbBr₃ QDs,^[29] and their water and light stability were significantly improved. But much more stable coatings using inorganic materials are preferred if possible. Zheng and co-workers prepared CsPbBr₃@TiO₂ core-shell nanocrystals, which presented super stability for three months storage in water with identical optical features remained. Whereas the crystallization process of TiO₂ required high temperature assist (300 °C), which resulted the quenching of perovskite QDs.^[30] Except these above materials, encapsulating QDs with silica shell has been recognized as one fantastic approach to improve the stability for perovskite QDs, because silica as an optical transparent, chemical inert, and nontoxic material can prevent the core materials from the release of toxic

ion as well as chemical degradation. Actually, coating perovskite QDs with silica has been widely investigated.^[31–33] All those silica coating composites not only maintain almost all the properties related with perovskite QDs but also achieve reduced chemical sensitivity and enhanced thermal and photostability. For example, the silica shell has improved the luminescent feature and prolonged the photostability of CH₃NH₃PbBr₃ QDs in both solution and powder forms.^[34] Our group further demonstrated that CsPbBr₃ QDs displayed enhanced emissive properties, as well as humidity and thermal stabilities through a well-defined structure of silica coating.^[35] Both studies have also revealed that employing silica shell can terminate the anion-exchange effect occurred in perovskite QDs with different halogens. These unique properties of silica coated perovskite QDs provide an idea to fabricate white LEDs by involving the mixture of red and green emitting QDs and a commercially available blue or UV chip.^[31]

Different approaches have been established for the preparation of SiO₂ coated perovskite QDs. Generally, only thick shell (50–100 nm) could be produced using traditional silica coating technology, and core-shell structured perovskite QDs in which only each individual QD is separately coated by silica was rarely reported. A thick shell will gather a large volume of QDs and induce QDs aggregation in one single SiO₂ sphere or a large size that may be bulkier than desired. As a result, most of the PL spectra were shifted and/or broadened, accompanied with reduced PLQY and surface scattering signal.^[31,36,37] Whereas an ultrathin silica shell that is thin enough coated on QDs has been demonstrated to be an effective way to avoid above defects and enhance luminescence features along with chemical stability.^[38] Great research efforts have been made to reduce the thickness of silica layer capped on QDs and the results are inspired. For example, Philipse et al. demonstrated that the thin layer of SiO₂ could be obtained by exposing the silica and QDs to a dilute alkaline solution of sodium silicate for 2 h.^[39] Hui et al. used citrate and nitrate salts as precursors and obtained hydrophilic citrate-capped Fe₃O₄ QDs.^[40] Both above methods rely on the use of either some sort of pretreatment or an appropriate additive for the uncoated QDs, which introduce additional steps and increase the complexity of the process. Joo et al. reported that the Pt@SiO₂ core-shell QDs can be prepared by changing the concentration of silane source.^[41] This strategy makes us aware of the possibility to obtain the ultrathin layer, monodispersed, core-shell structured silica coated perovskite QDs on the nanometer scale.

In this present work, we introduced a facile strategy for making monodispersed SiO₂ coated Mn²⁺ doped CsPbX₃ QDs (X = Br, Cl) via a versatile sol-gel method at room temperature. This method involves the hydrophilic groups of trioctyl-phosphine oxide (TOPO) and 2-methoxyethanol (2-ME), which are surfactants present on the QDs surface. Subsequently, a certain amount of tetraethoxysilane (TEOS) was selected as silica precursor for the production of SiO₂ shell. The SiO₂ shell of ≈2 nm can effectively passivate the CsPbMnX₃ QDs core, inducing a high PLQY of 50.5%, low toxicity, and admirable optical stability. More importantly, anion-exchange can be completely prevented after SiO₂ coating. Owing to those excellent properties, one promising white LED device was fabricated by using the CsPbMnX₃@SiO₂ and CsPbBr₃ QDs as novel luminescent



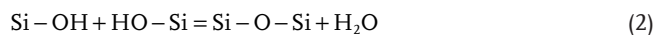
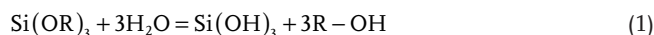
Scheme 1. Schematic illustration of the procedure for synthesizing CsPbMnX₃@SiO₂ core-shell QDs.

materials. The as-obtained white LED produced excellent-quality white light with a high luminous efficiency of 68.4 lm W⁻¹ and a high CRI of 91 at a driving current of 10 mA, guaranteeing their potential practical application.

2. Results and Discussion

The ultrathin, core-shell CsPbMnX₃@SiO₂ QDs were synthesized via two steps as schematically shown in **Scheme 1**. At the first step, we prepared CsPbMnX₃ QDs by using the emulsion and demulsion reprecipitation technology, which was usually adopted to fabricate pure organometal halide perovskite QDs.^[42] The N,N-dimethylformamide (DMF) precursor solution containing PbBr₂, PbCl₂, MnBr₂, and CsBr was injected into toluene at room temperature. In this process, orthorhombic CsPbMnX₃ QDs were formed. To reduce the hydrolysis reaction of TEOS, TOPO acting as surfactant was selected as ligands to modify the QDs's surface. Last, TEOS as silane was added to the obtained QDs solution. After hydrolysis reaction of TEOS, the SiO₂ layers were directly formed on QDs. As known to all, the ligands on the surface of QDs play a crucial role in the fabrication of SiO₂ coated QDs. For example, Selvan And Tan involve the oil group of TOPO and Igepal, which are surfactants present on the QDs surface to facilitate the formation of CdSe@SiO₂.^[43] In our previous work, TEOS acting as a single ligand was directly added in the CsPbBr₃ solution for the fabrication of CsPbBr₃/SiO₂ QDs, which shows a large amount of CsPbBr₃ QDs embedding into one silica sphere.^[35] This is because a large amount of TEOS would directly contact with water molecule, and this contact would accelerate hydrolysis reaction rate of TEOS. After being added with the oil group of TOPO in the

CsPbMnX₃ QDs solution, the interaction between the QDs and water molecule can be reduced and the hydrolysis reaction of TEOS can be sufficiently low. Besides, the presence of water molecule from air is sufficient to realize the hydrolysis reaction, and the 2-ME acting as a catalyst can help the achievement of Si-O-Si matrix around the QDs surface. Therefore, we can obtain the ultrathin, core-shell structured CsPbMnX₃@SiO₂ QDs. The reaction process includes the hydrolysis of silane precursor (Si(OR)₃) (Equation (1)) and oxolation of hydrolytic product after reaction with water (Equation (2))



After purification, the obtained products are dispersed in hexane and characterized. The elaborate experimental procedure is described in the Experimental Section.

Figure 1a,b present the typical transmission electron microscopy (TEM) and high resolution TEM (HRTEM) images of the obtained CsPbMnX₃ QDs, respectively, showing that the Mn element does not affect the crystal formation of perovskite QDs. The good dispersity of the CsPbMnX₃ QDs exhibits quasi square shaped with an average diameter of 11 ± 1.0 nm, which is similar with the undoped ones (Figure S1, Supporting Information). HRTEM observation reveals that the as-obtained QDs have legible crystal lattices with an interplanar distance of 5.69 Å. Representative TEM micrograph of the as-prepared core-shell structured CsPbMnX₃@SiO₂ QDs is presented in Figure 1c, where each Mn²⁺ doped perovskite QD is engaged within a silica shell, suggesting that the SiO₂ shell has isotropic

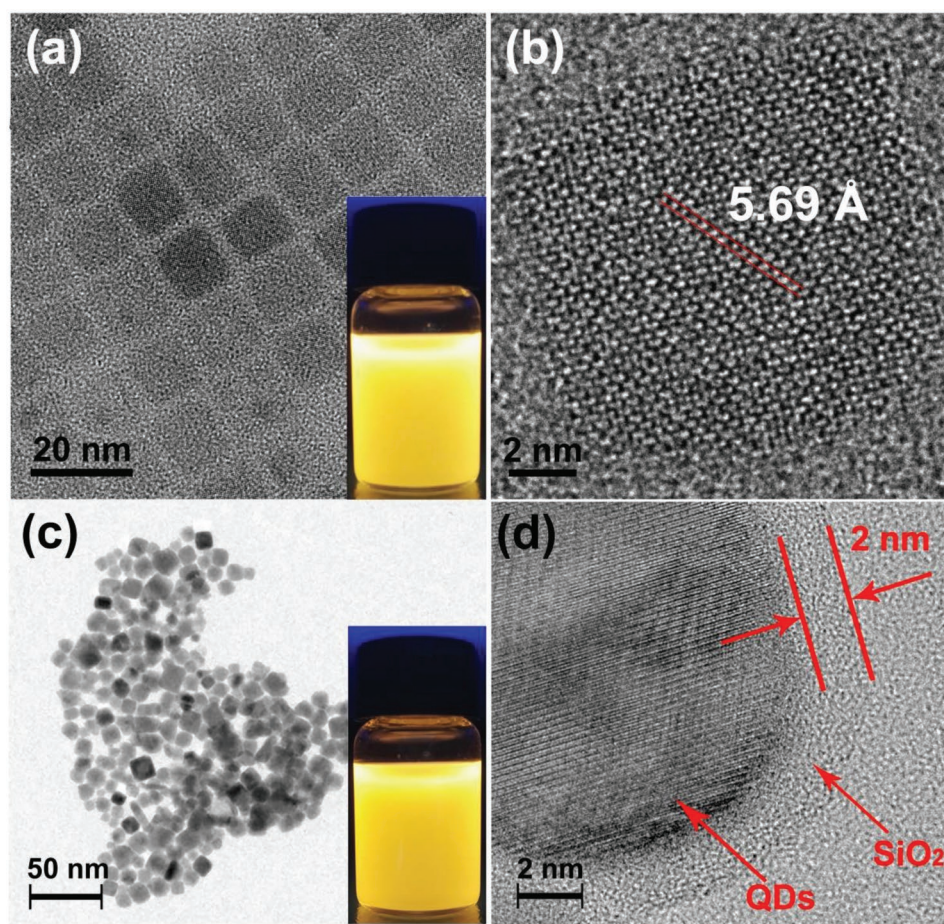


Figure 1. a) TEM and b) HRTEM micrographs of the typical CsPbMnX₃ QDs. c) Representative TEM and d) HRTEM micrographs of CsPbMnX₃ QDs individually encapsulated within SiO₂ shells. Inset of (a) and (c) are the photographs of pure and silica coated CsPbMnX₃ QDs dispersed in hexane illuminated by a UV lamp, respectively.

growth with slightly smooth surface. Compared with the emission of CsPbMnX₃ QDs (inset of Figure 1a), CsPbMnX₃@SiO₂ QDs solution shows the similar PL emission under UV light (inset of Figure 1c). The photograph of CsPbMnX₃ QDs shows an almost completely transparent toluene solution under room light (Figure S2, Supporting Information). While, it is worthy to note that the color of the CsPbMnX₃@SiO₂ QDs exhibits a slight milk-white color, and this phenomenon can be explained that the solubility of the SiO₂ coated QDs is worse than that of uncoated ones. HRTEM micrograph of CsPbMnX₃@SiO₂ QDs is shown in Figure 1d, the core–shell boundary can be clearly observed and the thickness of silica shell is measured to be ≈2 nm. The continuous lattice fringes throughout the whole QDs reveal their high crystallinity. In the meantime, the average diameter of these core–shell QDs is around 15 nm, which is apparently larger than the TEM observation of initial Mn²⁺ doped QDs. Moreover, no blur and breakage are observed in Figure 1d for the CsPbMnX₃ QDs core parts and their cubic morphology are completely preserved, indicating that the dissolution of CsPbMnX₃ QDs can be effectively avoided from the ammonia solution in silica. However, because of the surface properties of these QDs, the coated QDs cannot be remained homogeneous during the hydrolysis process of silane.

The as-prepared CsPbMnX₃@SiO₂ QDs were further characterized by using the X-ray energy dispersive spectroscopy (EDS) as shown in Figure 2a. Elements of caesium, lead, manganese, bromine, chlorine, silicon were clearly detected, which is in agreement with the provided components. The X-ray photoelectron spectroscopy characterization was also performed to explore the valence states of the constituent elements in the as-synthesized CsPbMnX₃@SiO₂ QDs (Figure S3, Supporting Information). It could be confirmed that the valence of the QDs elements are Cs⁺, Pb²⁺, Br⁻, Cl⁻, and Mn²⁺, and the Si 2p peak appeared due to the presence of SiO₂ shell layer. In the survey-scan of Fourier transform infrared spectroscopy spectrum of the final obtained CsPbMnX₃@SiO₂ QDs (Figure S4, Supporting Information), peaks appeared at 1125 and 960 cm⁻¹ due to Si–O–Si vibrations and Si–OH twisting vibration, respectively, indicating the hydrolysis condensation of TEOS and demonstrating the formation of a cross-linked silica matrix. Figure 2b depicts the X-ray diffraction (XRD) patterns of CsPbMnX₃ and core–shell CsPbMnX₃@SiO₂ QDs, and both of the two samples belong to the same orthorhombic CsPbX₃ phase (JCPDS 54–0752), verifying the silica layer has almost no impact on the crystallinity of perovskite. In addition, the peak intensity ratio of (200) at 32° and (110) at 23.1° changes from ≈1.07 in CsPbMnX₃

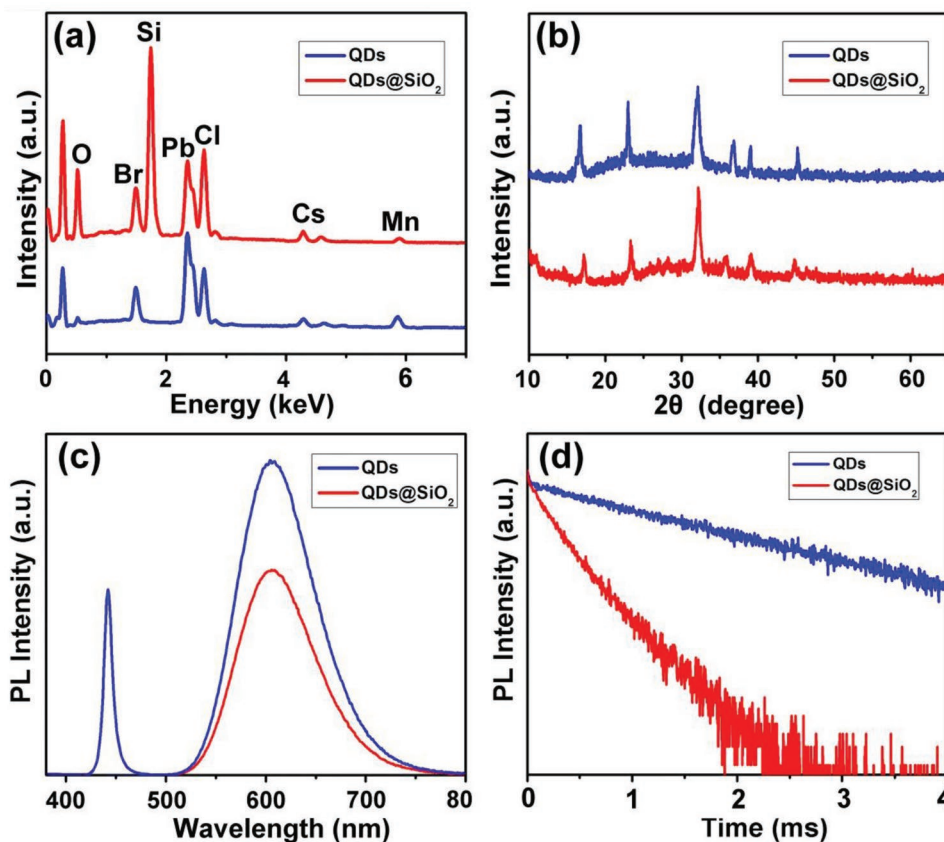


Figure 2. a) EDS spectra, b) XRD patterns, c) PL spectra, and d) PL lifetime decays of Mn^{2+} emission for the CsPbMnX_3 QDs (blue lines) and $\text{CsPbMnX}_3@SiO_2$ QDs (red lines), respectively. Note: the PL spectra of the two samples in (c) are normalized, and the spectrum of $\text{CsPbMnX}_3@SiO_2$ QDs is overlapping with the one of CsPbMnX_3 QDs.

QDs to 1.53 for $\text{CsPbMnX}_3@SiO_2$ QDs, and the slight increased relative peak intensity of (200) diffraction for $\text{CsPbMnX}_3@SiO_2$ QDs suggests the growth of the QDs along the (200) plane.^[44] It should be noted that in the presented work the solution processing method can be recognized as one of the most efficient approaches to prepare $\text{CsPbMnX}_3@SiO_2$ core-shell QDs. However, this approach is usually accompanied by material inhomogeneity, and some of the CsPbMnX_3 particles are grown up (Figure 1c), which may result in the changes of diffraction peaks intensity in their XRD pattern. The normalized PL spectra of the above two samples are displayed in Figure 2c. Compared with the PL spectrum of the CsPbMnX_3 QDs, no obvious shift for the PL peaks of $\text{CsPbMnX}_3@SiO_2$ QDs is observed. Considering that QDs aggregation and interdot energy transfer will lead to a shift of PL peaks, our result demonstrates good dispersibility and suppressed aggregation of QDs in SiO_2 shell, which can separate the perovskite QDs individually. Additionally, owing to the contribution of passivation effect from SiO_2 , the relative emission intensity at 607 nm is decreased as compared to the uncoated QDs. The PLQY of SiO_2 coated CsPbMnX_3 QDs is found to be a slightly lower (50.5%) than that of the corresponding uncoated CsPbMnX_3 QDs (54.7%). This result can be manifested by a faster exciton decay as illustrated in Figure 2d for Mn^{2+} emission decay and Figure S5 in the Supporting Information for exciton emission decay. Comparison of the Mn^{2+}

doped CsPbX_3 QDs, significant change in the fluorescence lifetimes after coating has been observed both for the excitonic PL located at 446 nm and the Mn^{2+} PL located at 607 nm. The $\text{CsPbMnX}_3@SiO_2$ QDs show a shorter average PL lifetimes (15.7 ns for excitonic emission and 0.7 ms for Mn^{2+} emission (Tables S1 and S2, Supporting Information)) than the Mn^{2+} doped CsPbX_3 QDs (23.5 ns for excitonic emission and 0.82 ms for Mn^{2+} emission), indicating that the addition of TEOS can remove the surface ligands during the hydrolysis process of silane and leads to a presence of surface traps and additional nonradiative channels resulting from them.

On the basis of the aforementioned analyzation, an essential process is required to penetrate into the fundamental formation process of the novel core-shell SiO_2 coated CsPbMnX_3 QDs. Therefore, the reaction system for synthesizing $\text{CsPbMnX}_3@SiO_2$ QDs with different proportion of TEOS was examined. By content-dependent TEM studies, the morphology of this type of QDs can be controlled. If the content of TEOS is decreased to 100 μL compared with the amount required for the optimized condition of 200 μL , the silica shell cannot be formed and large amount of amorphous silica existed (Figure 3a). Increasing the TEOS content to 200 μL , core-shell structure is formed and each CsPbMnX_3 QDs is exactly incorporated in one SiO_2 (Figure 3b). When the amount of TEOS is increased to 300 μL , the formation of $\text{CsPbMnX}_3@SiO_2$ QDs and amorphous silica

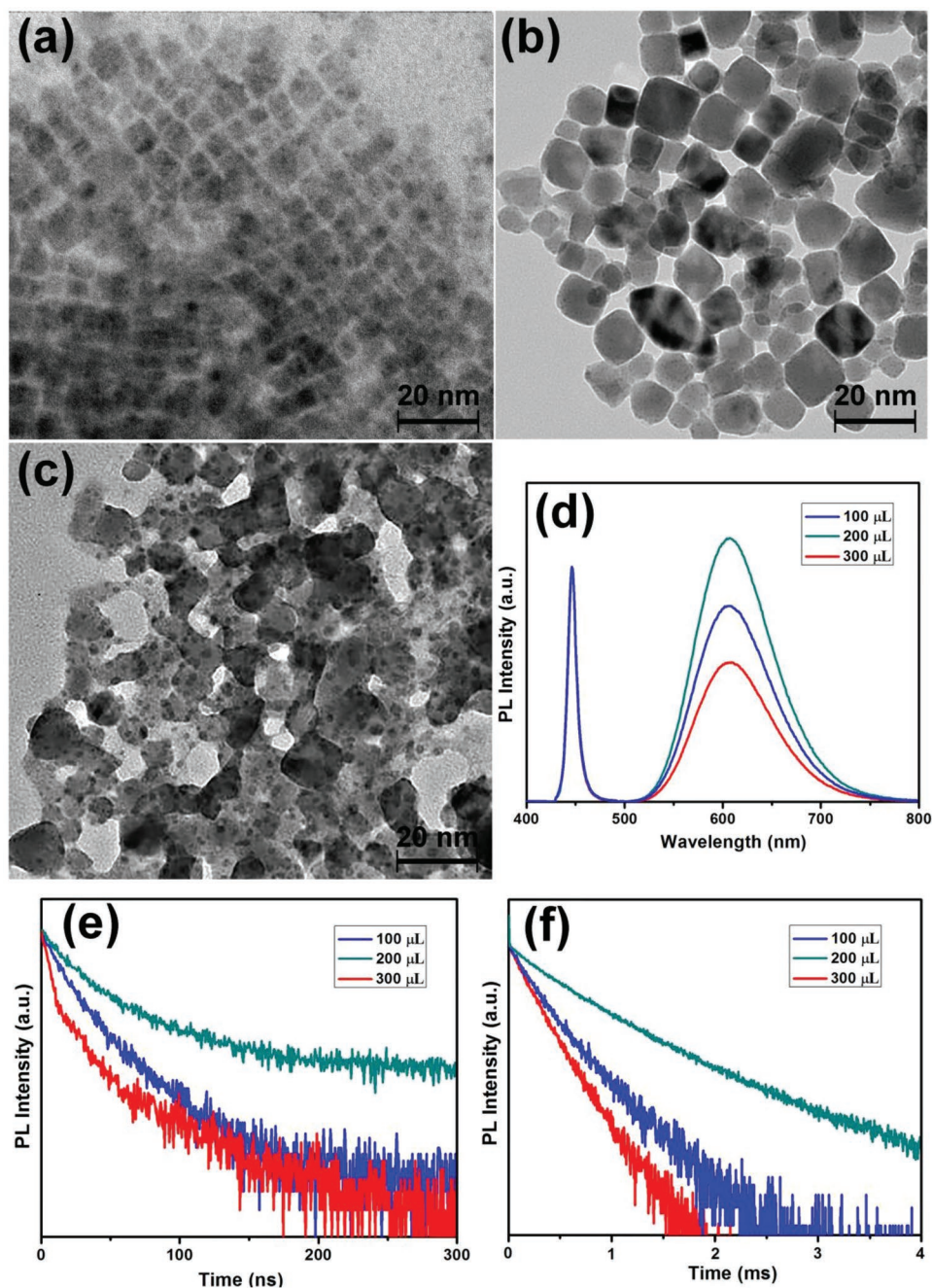


Figure 3. TEM images of product prepared at different TEOS contents: a) 100 μL , b) 200 μL , and c) 300 μL . d) Corresponding PL spectra and e) time-resolved PL lifetimes for e) the excitonic emission decay and f) Mn^{2+} emission decay of the as-obtained $\text{CsPbMnX}_3@SiO_2$ QDs. Note: the PL spectra of the three samples in (d) are normalized, and the spectra of $\text{CsPbMnX}_3@SiO_2$ (200 μL) and $\text{CsPbMnX}_3@SiO_2$ (300 μL) QDs are overlapping with the one of $\text{CsPbMnX}_3@SiO_2$ (100 μL) QDs.

in TEM image is observed as shown in Figure 3c. For the content of TEOS to 400 μL , huge SiO_2 microsphere containing a large amount of CsPbMnX_3 QDs is obtained (Figure S6, Supporting Information), and this configuration is consistent with our previous report about $\text{CsPbBr}_3@SiO_2$ nanocrystals.^[35] The PL features of $\text{CsPbMnX}_3@SiO_2$ QDs were collected to explore the silane effect. As shown in Figure 3d, varying the content of TEOS does not effect the peaks location for the obtained

$\text{CsPbMnX}_3@SiO_2$ QDs. However, after the excitonic emission intensity is normalized, the relative intensities of Mn^{2+} emission were decreased along with the TEOS added. Meanwhile, the emission colors under UV excitation were changed from brilliant yellow for uncoated QDs to dark yellow (100 μL), brilliant yellow (200 μL), and dark yellow (300 μL) (Figure S7, Supporting Information). This phenomenon can be explained that SiO_2 could restrain the activated nonradiative deactivation

of Mn^{2+} and exciton emissions in the CsPbX_3 QDs.^[45] The absolute PLQYs of 54.7%, 47.9%, 50.5%, and 33.5% for the pure CsPbMnX_3 , $\text{CsPbMnX}_3@/\text{SiO}_2$ (100 μL), $\text{CsPbMnX}_3@/\text{SiO}_2$ (200 μL), and $\text{CsPbMnX}_3@/\text{SiO}_2$ (300 μL), respectively, are obtained. The highest PLQY is ascribed to the lowest trapping possibility of excitons and least defects. When the content of TEOS is less than 200 μL , a small quantity of inorganic silica for covering the dangling bonds is deficient and defects exposed on the surface of the CsPbMnX_3 QDs are existing, thus the PLQY is reduced. Whereas, if the content of TEOS is more than 200 μL , large amount of TEOS connected with the QDs surface leads to the formation of spatial steric hindrance, which results from the hydrolysis of TEOS strengthening, and such steric hindrance can bring on defects, thus PLQY declines.^[46,47]

To further investigate the defects passivation effect of silane on PL behaviors of the $\text{CsPbMnX}_3@/\text{SiO}_2$ QDs, fluorescence lifetimes of the coated QDs obtained at different TEOS contents in the range of 100–300 μL were characterized. The PL lifetime curves are presented in Figure 3e for the excitonic emission at 446 nm and Figure 3f for the Mn^{2+} emission at 607 nm. In general, the PL relaxation of the three samples can be described by an equation: $I(t) = A_1 \exp(-t/\tau_1) + A_2 \exp(-t/\tau_2)$, where τ_1 and τ_2 represent the decay time of the PL emission and A_1 and A_2 are the fractional contributions of the decay components. The PL relaxations can be decomposed into fast and slow decay components. The mean lifetime (τ_{avg}) can be determined according to the equation: $\tau_{\text{avg}} = \frac{A_1 \tau_1^2 + A_2 \tau_2^2}{A_1 \tau_1 + A_2 \tau_2}$. The fitting and calculated results are displayed in Tables S3 and Table S4 in the Supporting Information for excitonic emission decay and Mn^{2+} emission decay, respectively.

For the $\text{CsPbMnX}_3@/\text{SiO}_2$ (100 μL), $\text{CsPbMnX}_3@/\text{SiO}_2$ (200 μL), and $\text{CsPbMnX}_3@/\text{SiO}_2$ (300 μL), the excitonic decay times are ($\tau_1 = 5.6$ ns, $\tau_2 = 17.1$ ns), ($\tau_1 = 7.7$ ns, $\tau_2 = 20.6$ ns), and ($\tau_1 = 1.86$ ns, $\tau_2 = 12.8$ ns), respectively, the Mn^{2+} emission decay times are ($\tau_1 = 0.27$ ms, $\tau_2 = 0.66$ ms), ($\tau_1 = 0.32$ ms, $\tau_2 = 0.92$ ms), and ($\tau_1 = 0.13$ ms, $\tau_2 = 0.62$ ms), respectively. The average lifetimes for the excitonic decay times are 11.3, 15.7, and 7.9 ns, respectively, and for Mn^{2+} emission decay times are 0.5, 0.7, and 0.21 ms, respectively. It is observed that using 200 μL TEOS to prepare $\text{CsPbMnX}_3@/\text{SiO}_2$ QDs exhibits a longer lifetime. The PL lifetime is decreased for the $\text{CsPbMnX}_3@/\text{SiO}_2$ (100 μL) QDs, and further decreased for $\text{CsPbMnX}_3@/\text{SiO}_2$ (300 μL) QDs. The long lifetime (200 μL) usually indicates that the nonradiative decay is suppressed, which is beneficial for the recombination of the generated excitons and results in a high PLQY. All those results demonstrate that the concentration of TEOS plays a crucial role in controlling the morphology and optical properties of $\text{CsPbMnX}_3@/\text{SiO}_2$ QDs.

For practical application in photoelectronic devices such as white LEDs, thermostability issue of perovskite QDs is one of most significant factors needed to be considered, since the obtained QDs would suffer from high temperatures during LEDs working. We first measured the surface temperatures of GaN LED chip under different driving currents as presented in Figure S8 in the Supporting Information. When the operating current is 200 mA, the surface temperature of the LED chip reaches 67.4 °C. Thus, we investigated the optical features of CsPbMnX_3 QDs and $\text{CsPbMnX}_3@/\text{SiO}_2$ QDs films and both

were annealed at 67 °C under vacuum condition for 1 h. It can be found that the PL intensity of Mn^{2+} emission is decreased after the uncoated QDs annealed (down to 73%) (Figure S9a, Supporting Information). Nevertheless, the Mn^{2+} emission of $\text{CsPbMnX}_3@/\text{SiO}_2$ QDs could maintain as high as $\approx 95\%$ of their initial intensity (Figure S9b, Supporting Information). It is known that GaN chips with different model may exhibit different surface temperatures, and high annealing temperatures can result in PL quenching.^[48,49] For the preservation of the perovskite QDs, the annealed temperatures were often less than 50 °C.^[50] It is generally accepted that silica matrix can act as buffer to effectively prevent damage from thermal effect, which is associated with a more dense structure of SiO_2 . Therefore, a high experimental temperature (for example, 100 °C) is essential to explore their thermal stability for perovskite NCs.^[31,51] Based on this, we investigated the optical features of CsPbMnX_3 QDs and $\text{CsPbMnX}_3@/\text{SiO}_2$ QDs films and both were annealed at 100 °C under vacuum condition for 1 h. The PL intensity of CsPbMnX_3 QDs film was obviously decreased (down to 50%) (Figure 4a). Whereas the emission of the $\text{CsPbMnX}_3@/\text{SiO}_2$ films could maintain as high as $\approx 90\%$ of their initial intensity (Figure 4b). In addition, slight red shift was presented for the PL peaks location of CsPbMnX_3 QDs after thermal annealing, which was caused by the crystal growth or aggregation of QDs. By contrast, with the protection provided by SiO_2 shell showed almost no red shift for the PL peak of $\text{CsPbMnX}_3@/\text{SiO}_2$ QDs, which demonstrated a higher thermal stability for the $\text{CsPbMnX}_3@/\text{SiO}_2$ QDs in comparison to the CsPbMnX_3 QDs.

To evaluate the stability related to water resistance, CsPbMnX_3 and $\text{CsPbMnX}_3@/\text{SiO}_2$ QDs powders were dispersed in water and then stirred for six days. Color and PLQY variation for both two samples were recorded. As illustrated in Figure 4c, the bright emission for uncoated CsPbMnX_3 QDs was sharply dropped along with the storage time and completely disappeared after 6 days stirring (top four pictures). By contrast, the orange-yellow light emission from the SiO_2 modified CsPbMnX_3 QDs in water solution presented almost no change after being stored for 6 days (bottom four pictures). The PLQY of $\text{CsPbMnX}_3@/\text{SiO}_2$ QDs can maintain $\approx 90\%$ of the initial efficiency even being stored for 6 days in water (Figure 4d). While the PLQY for the CsPbMnX_3 QDs is obviously decreased in the first day and almost declined to zero after storage for 6 days. The XRD patterns of the two samples have been recorded after 1 min and 6 days storage. The crystal structure of CsPbMnX_3 QDs was completely deteriorated and the corresponding XRD signal was almost disappeared after being stored with these QDs in water for six days (Figure S10, Supporting Information). On the contrary, $\text{CsPbMnX}_3@/\text{SiO}_2$ QDs exhibited much higher stability in water. As presented in Figure S11 in the Supporting Information, only a slight decrease of the intensity of XRD signal can be observed, and all the characteristic peaks belong to perovskite can be specifically determined, verifying the excellent water stability of $\text{CsPbMnX}_3@/\text{SiO}_2$ QDs in water. We have reported that the water stability of the Mn^{2+} doped CsPbX_3 QDs is much higher than the undoped ones.^[52] TEM images of CsPbMnX_3 and $\text{CsPbMnX}_3@/\text{SiO}_2$ QDs during and after the 6 days in water are provided. As displayed in Figure S12 in the

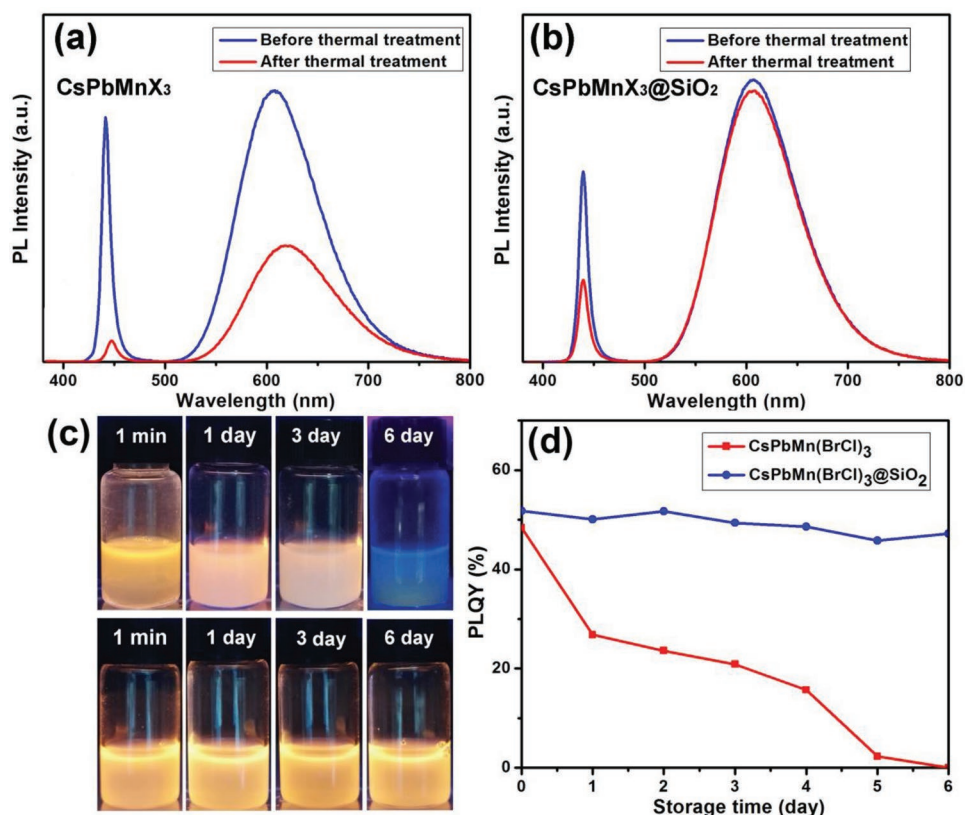


Figure 4. PL spectra of a) CsPbMnX₃ and b) CsPbMnX₃@SiO₂ QDs before and after thermal treatment at 100 °C for 1 h. c) The photographs of CsPbMnX₃ and CsPbMnX₃@SiO₂ QDs in water solution under UV light; the pictures were taken once a day (the top four for pure CsPbMnX₃ QDs and the bottom four for CsPbMnX₃@SiO₂ QDs). d) The PLQY changes of the CsPbMnX₃ and CsPbMnX₃@SiO₂ QDs.

Supporting Information, CsPbMnX₃ QDs with gradual degradation in water can be clearly seen. On the contrary, TEM images of CsPbMnX₃@SiO₂ QDs with basic morphology are maintained during storage in water for six days (Figure S13, Supporting Information). While, the size of some of the QDs is obviously increased in the first day and further increased to 100 nm after storage for 6 days. The reason for the QD's size increase and QD's shape evolution can be explained by the interaction between the QDs and water. Even though the SiO₂ is fully covered on the QDs surface, minor amounts of H₂O molecules can still be in contact with the QDs due to their long time soaking and stirring in water. Water molecule as a polar solvent can help to activate the QDs surface by replacing their surface capping ligands (oleic acid (OA), *n*-octylamine (OLE), and TOPO) with H₃O⁺ and OH⁻, which are ionized from water with the help of OA (or OLE, TOPO).^[53] It has been reported that the length of the adopted ligands can affect the growth of QDs. For example, Deng and co-workers have demonstrated that CsPbBr₃ QDs, nanocubes, nanorods, and nanowires can be fabricated by employing different acid and amine ligands.^[54] Here, H₃O⁺ and OH⁻ ions can act as surface ligands and influence the growth orientation of perovskite QDs to form nanoplatelets.^[55] Besides, these QDs are still coated by a thin SiO₂ layer. The result indicates that the silica as protective shell achieves effective protection for the CsPbMnX₃ QDs from water and thus presents ultrahigh water stability.

In a further experiment for fabricating traditional white LEDs, the QDs composite solution containing green and red emissive QDs is deposited on a commercially available UV/blue LED chip. On account of the ion exchange effect of halogen elements in perovskite QDs, the perovskite QDs cannot be simply mixed as cadmium-based QDs do. The spectra of green CsPbBr₃ QDs and the CsPbMnX₃ QDs under excitation are presented in Figure 5a. The peak at 500 nm is from CsPbBr₃ QDs (seagreen line, basic morphology, and optical features are shown in Figure S14 in the Supporting Information), and that at 446 and 607 nm are from CsPbMnX₃ QDs (purple line). Their mixture spectrum is also illustrated in Figure 5a (blue line). The blue and green spectrum regions strongly shift to one cyan region. Besides, the relative intensity of the peak at 607 nm is suppressed and that leads to the cyan emission (inset of Figure 5a). Due to the strong ion-exchange effect, these pure QDs cannot be applied on white LED devices. Subsequently, green CsPbBr₃ QDs were mixed with CsPbMnX₃@SiO₂ QDs to avoid the ion-exchange effect. The resulted spectra are presented in Figure 5b. No spectra shift occurred and the spectral shapes were perfectly preserved, indicating that the ion-exchange effect has been completely blocked with the isolation by SiO₂. Thus, we obtained the white emissive mixture QDs (inset of Figure 5b). Taken together, all these advantages suggest that the CsPbMnX₃@SiO₂ QDs have great potential applications in practical lightings and displays.

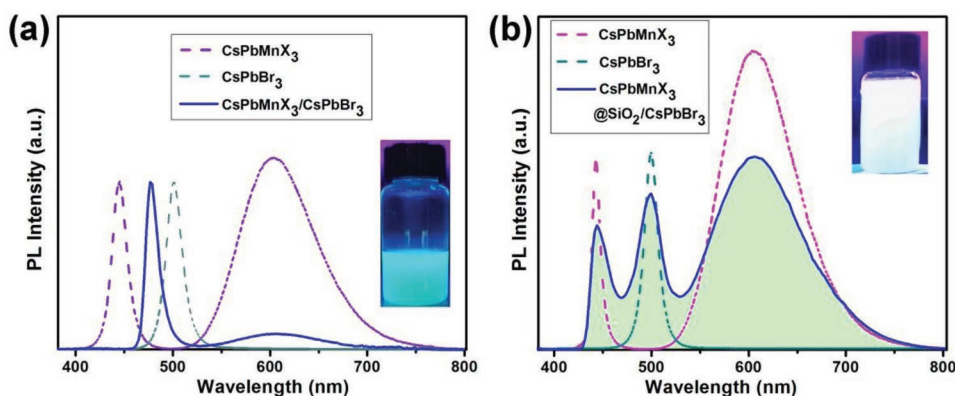


Figure 5. a) PL spectra of CsPbBr₃ QDs (seagreen), CsPbMnX₃ QDs (purple), and mixture of them (blue) under UV light excitation. Inset: cyan emissive photograph of CsPbBr₃ and CsPbMnX₃ QDs mixture under UV light. b) PL spectra of CsPbBr₃ QDs (seagreen), CsPbMnX₃@SiO₂ QDs (pink), and mix of them (blue) under UV light. Inset: white emissive photograph of CsPbBr₃ and CsPbMnX₃@SiO₂ QDs mixture under UV light.

Although it was recently reported that the perovskite QDs were used to fabricate white LEDs, many researchers relied on the combination of green emitting CsPbBr₃ QDs with red-emitting Cd-based QDs or commercial phosphor (K₂SiF₆Mn⁴⁺).^[56,57] Our SiO₂ coated Mn²⁺ doped perovskite QDs are suitable for the generation of warm white LEDs, because they have dual emission spectra of blue and yellow colors and can effectively prevent ion exchange by the presence of SiO₂. Therefore, The white emissive mixture of CsPbMnX₃@SiO₂ and CsPbBr₃ QDs can be directly utilized as phosphor casting on a UV GaN LED for the preparation of white LED device. **Figure 6a** presents the EL spectra of the fabricated white LED, which are recorded under different driving currents and display no saturation

characteristic. Besides, ascribing to the thermal quenching effect of QDs, the color coordinate shows a slight shift to blue region with the driving current increasing (Figure 6b). It well known that the increase of forward current comes with the rise of chip temperature, and this raise could lead to thermal quenching for the emissive QDs. Figure 6c depicts the luminous efficiency variation with the increasing forward current from 10 to 200 mA. The attained maximum luminous efficiency is 68.4 lm W⁻¹ at 10 mA. The efficiency is decreased gradually with the increase of the forward current (from 68.4 lm W⁻¹ at 10 mA to 41.9 lm W⁻¹ at 200 mA). This decreasing trend is caused by the combining effects of thermal degradation of green and yellow emissive QDs and the intrinsic efficiency drop of the blue LED chip

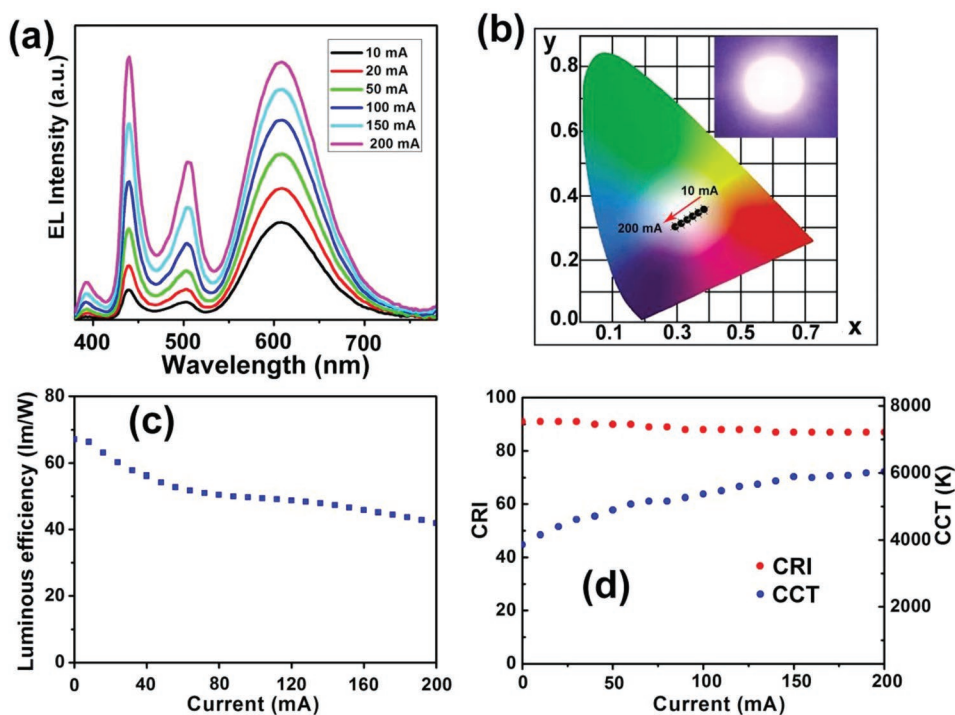


Figure 6. Evolution of a) EL spectra, b) CIE color coordinates, c) luminous efficiency, and d) CRI and CCT of the white LED device under different driving currents ranging from 10 to 200 mA. Inset of (b) shows a digital camera image of the fabricated white LED device under forward current of 20 mA.

itself. Figure 6d illustrates the detailed CRI values and correlated CCT variation under different driving currents. Values of CCT increase from 3857 K at 10 mA to 5934 K at 200 mA, and this variation is in consistence with the shift of CIE color coordinates. Small changes of CRI are observed (from 91 to 87) in the range of applied current, which suggests a high stability of the obtained white LED device against the current variations. These results will further promote the applied progress of CsPbMnX₃@SiO₂ QDs in some fields such as display and solid-state lighting.

3. Conclusions

To summarize, we have successfully presented a facile synthetic route to prepare the ultrathin, core-shell structured Mn²⁺ doped CsPbX₃ QDs coated by ultrathin SiO₂ layer at room temperature for the first time. The SiO₂ morphology was systematically investigated and optimized to achieve a highest PLQY of 50.5%. Thermal stability and water resistance results suggest that the CsPbMnX₃@SiO₂ QDs were notably stable than the uncoated ones. Besides, after mixing CsPbMnX₃@SiO₂ with CsPbBr₃ QDs solution, we can obtain white emissive QDs composite solution. We further used the composite integrated with a UV LED chip to fabricate white LED device, which displayed excellent-quality white light with a high CRI value of ≈91 and a luminous efficiency of 68.4 lm W⁻¹ at a forward current of 10 mA. We anticipate that our present work can be further applied in myriad areas such as biological imaging, medical diagnosis, and optoelectronic devices.

4. Experimental Section

Materials: CsBr (99.9%, from Xi'an Polymer Light Technology Corp.), PbBr₂ (99%, from Xi'an Polymer Light Technology Corp.), PbCl₂ (99%, from Xi'an Polymer Light Technology Corp.), MnBr₂·(H₂O)₄ (98%, from Aladdin-reagent), DMF (99%, from Aladdin-reagent), OLE (98%, from Aladdin-reagent), OA (90%, from Aladdin-reagent), 2-ME (98%, from Aladdin-reagent), dimethyl sulfoxide (DMSO, 99.7%, from Aladdin-reagent), TOPO (95%, from Aladdin-reagent), and TEOS (99%, from Aladdin-reagent) were used. All the chemicals were used as received.

Preparation of CsPbBr₃ QDs: CsPbBr₃ QDs were synthesized following previously reported procedures.^[5] Briefly, the precursor solution was prepared by mixing 0.4 mmol of PbBr₂, 0.4 mmol of CsBr, 1 mL of DMF, 1.5 mL of OA, and 0.25 mL of OLE. Then, 10 mL of toluene was added dropwise into the precursor solution with vigorous stirring. Green emission was observed immediately under 365 nm ultraviolet light after the injection.

Preparation of Mn²⁺ Doped CsPbMnX₃ QDs: MnBr₂/PbX₂-DMSO composite was first prepared by mixing 0.4 mmol PbX₂ (PbBr₂:PbCl₂ = 1:1), 0.8 mmol MnBr₂, and 2 mL DMSO with vigorous stirring for 12 h. Then, toluene solution (20 mL) was added. After centrifugation, the obtained white powder (MnBr₂/PbX₂-DMSO) was dried at 80 °C for 12 h. For the synthesis of Mn²⁺-doped CsPbX₃ QDs, the aforementioned MnBr₂/PbX₂-DMSO composite and 0.4 mmol of CsBr were dissolved in 10 mL DMF with 1 mL of OA and 0.5 mL of OLE. The mixture was vigorously stirred to a clear solution. Upon mixing with toluene, yellow emissive QDs solution under 365 nm ultraviolet light was observed.

Preparation of the SiO₂ Coated CsPbMnX₃ QDs: To obtain the best result of CsPbMnX₃@SiO₂ QDs, we examined the effect of TEOS contents in our work. The content of TEOS should be calculated precisely. The molar mass and density of the TEOS are 208.33 g mol⁻¹

and 0.94 g mL⁻¹, respectively. For the sake of simple calculations, we assume that the QD's surface is completely covered by the silane, and no condensation or steric hindrance was considered. We assume that the obtained SiO₂ is cubic, from which its edge length and surface area can be derived. Separately, the volume and surface area of a single CsPbMnX₃ QD with cubic shape can be determined by its edge length (11 nm). Thus, we can yield the amount of silane demanded to coat the QDs with one monolayer. First, 1 mL TOPO and 500 μL 2-ME were added into 5 mL of the CsPbMnX₃ QDs (≈6 mg mL⁻¹) solution in a three-necked flask, then the mixture solution was stirred for 30 min under room temperature. Then, 200 μL TEOS was added without sealing and stirred for another 30 min in the air with temperature of 25 °C and relative humidity of 65%. After that, the obtained QDs solution was centrifuged for 10 min at 8000 rpm and the precipitate was collected.

Preparation of White LED Device: To fabricate the white LED devices, a GaN blue LED (λ_{max} = 392 nm) was used as an excitation source, and CsPbBr₃ QDs with green emission and CsPbMnCl₃@SiO₂ with yellow emission solutions in chloroform were blended with silicone binder and stirring. A hot plate (70 °C) was used to evaporate the chloroform. Subsequently, the final mixture was dropped on the top of the GaN LED. The device was further thermally annealed at 60 °C. After 1 h, the temperature was raised to 150 °C for another 1 h.

Characterizations: PL spectroscopy was obtained by a fluorescence spectrophotometer (PL: Agilent Cary Eclipse, Australia), which includes a Xe lamp as an excitation source with optical filters). Absorption spectrum was measured by a scan UV-vis spectrophotometer (UV-vis: UV-2100, Shimadzu, Japan). PLQY measurements were performed by Edinburgh fluorescence spectrometer FS 5. TEM was recorded using a ZEISS LIBRA200FE microscope. XRD patterns were characterized by Shimadzu/6100 X-ray diffractometer, using a Cu Kα radiation source with wavelength at 1.5405 Å. The properties of white LED were collected by a PR-670 Spectra Scan spectrophotometer (Photo Research).

Supporting Information

Supporting Information is available from the Wiley Online Library or from the author.

Acknowledgements

This work was supported by the National Natural Science Foundation of China (Grant Nos. 61520106012, 61475169, and 61674023), Chongqing Research Program of Basic Research and Frontier Technology (Grant No. cstc2017jcyjB0127), 100 Talents Program of Chinese Academy of Sciences (CAS), Strategic Priority Research Program of CAS (Grant No. XDB1603), International S&T Cooperation Program of China (Grant No. 2016YFE0119300), the Fundamental Research Funds for the Central Universities (Grant Nos. 106112017CDJQJ128837, 10611CDJXZ238826, and 2018CDYJSY0055), the Basic and Advanced Technology Research Project of Chongqing Municipality (Grant No. cstc2016jcyjA0371), the Scientific and Technological Research Foundation of Chongqing Municipal Education Commission (Grant No. KJ1600447), the Open Fund of the State Key Laboratory of High Field Laser Physics (Shanghai Institute of Optics and Fine Mechanics), Key Lab of Modern Optical Technologies of Education Ministry of China, Key Lab of Advanced Optical Manufacturing Technologies of Jiangsu Province, and Priority Academic Program Development (PAPD) of Jiangsu Higher Education Institutions.

Conflict of Interest

The authors declare no conflict of interest.

Keywords

core–shells, Mn²⁺-doping, quantum dots, SiO₂-coating, white light-emitting diodes

Received: January 28, 2019

Revised: March 14, 2019

Published online:

- [1] E. F. Schubert, J. K. Kim, *Science* **2005**, 308, 1274.
- [2] H. V. Demir, S. Nizamoglu, T. Erdem, E. Mutlugun, N. Gaponik, A. Eychmüller, *Nano Today* **2011**, 6, 632.
- [3] Q. Dai, C. E. Duty, M. Z. Hu, *Small* **2010**, 6, 1577.
- [4] S. Lee, J. Y. Hong, J. Jang, *ACS Nano* **2013**, 7, 5784.
- [5] T. Otto, M. Müller, P. Mundry, V. Lesnyak, H. V. Demir, N. Gaponik, A. Eychmüller, *Nano Lett.* **2012**, 12, 5348.
- [6] E. Jang, S. Jun, H. Jang, J. Lim, B. Kim, Y. Kim, *Adv. Mater.* **2010**, 22, 3076.
- [7] H. M. Zhu, C. C. Lin, W. Q. Luo, S. T. Shu, Z. G. Liu, Y. S. Liu, J. T. Kong, E. Ma, Y. G. Cao, R.-S. Liu, X. Y. Chen, *Nat. Commun.* **2014**, 5, 4312.
- [8] M. A. Becker, R. Vaxenburg, G. Nedelcu, P. C. Sercel, A. Shabaev, M. J. Mehl, J. G. Michopoulos, S. G. Lambrakos, N. Bernstein, J. L. Lyons, T. Stöferle, R. F. Mahrt, M. V. Kovalenko, D. J. Norris, G. Rainò, A. L. Efros, *Nature* **2018**, 553, 189.
- [9] A. Swarnkar, A. R. Marshall, E. M. Sanehira, B. D. Chernomordik, D. T. Moore, J. A. Christians, T. Chakrabarti, J. M. Luther, *Science* **2016**, 354, 92.
- [10] Y. Wang, X. Li, X. Zhao, L. Xiao, H. Zeng, H. Sun, *Nano Lett.* **2016**, 16, 448.
- [11] X. Li, Y. Wu, S. Zhang, B. Cai, Y. Gu, J. Song, H. Zeng, *Adv. Funct. Mater.* **2016**, 26, 2584.
- [12] J. Song, J. Li, X. Li, L. Xu, Y. Dong, H. Zeng, *Adv. Mater.* **2015**, 27, 7162.
- [13] L. Protesescu, S. Yakunin, M. I. Bodnarchuk, F. Krieg, R. Caputo, C. H. Hendon, R. X. Yang, A. Walsh, M. V. Kovalenko, *Nano Lett.* **2015**, 15, 3692.
- [14] A. Babayigit, A. Ethirajan, M. Müller, B. Conings, *Nat. Mater.* **2016**, 15, 247.
- [15] Y. Zhang, J. Liu, Z. Wang, Y. Xue, Q. Ou, L. Polavarapu, J. Zheng, X. Qi, Q. Bao, *Chem. Commun.* **2016**, 52, 13637.
- [16] M. Leng, Z. Chen, Y. Yang, Z. Li, K. Zeng, K. Li, G. Niu, Y. He, Q. Zhou, J. Tang, *Angew. Chem., Int. Ed.* **2016**, 55, 15012.
- [17] W. Stam, J. J. Geuchies, T. Altantzis, K. H. W. Bos, J. D. Meeldijk, S. V. Aert, S. Bals, D. Vanmaekelbergh, C. M. Donega, *J. Am. Chem. Soc.* **2017**, 139, 4087.
- [18] T. C. Jellicoe, J. M. Richter, H. F. J. Glass, M. Tabachnyk, R. Brady, S. E. Dutton, A. Rao, R. H. Friend, D. Credginton, N. C. Greenham, M. L. Böhm, *J. Am. Chem. Soc.* **2016**, 138, 2941.
- [19] A. Nag, S. Chakraborty, D. D. Sarma, *J. Am. Chem. Soc.* **2008**, 130, 10605.
- [20] B. B. Srivastava, S. Jana, N. S. Karan, S. Paria, N. R. Jana, D. D. Sarma, N. Pradhan, *J. Phys. Chem. Lett.* **2010**, 1, 1454.
- [21] D. Parobek, B. J. Roman, Y. Dong, H. Jin, E. Lee, M. Sheldon, D. H. Son, *Nano Lett.* **2016**, 16, 7376.
- [22] H. Huang, B. Chen, Z. Wang, T. F. Hung, A. S. Susha, H. Zhong, A. L. Rogach, *Chem. Sci.* **2016**, 7, 5699.
- [23] W. Xu, F. Li, F. Lin, Y. Chen, Z. Cai, Y. Wang, X. Chen, *Adv. Opt. Mater.* **2017**, 5, 1700520.
- [24] X. Li, M. I. Dar, C. Yi, J. Luo, M. Tschumi, S. M. Zakeeruddin, M. K. Nazeeruddin, H. Han, M. Grätzel, *Nat. Chem.* **2015**, 7, 703.
- [25] F. Palazon, Q. A. Akkerman, M. Prato, L. Manna, *ACS Nano* **2016**, 10, 1224.
- [26] X. Li, X. Zhong, Y. Hu, B. Li, Y. Sheng, Y. Zhang, C. Weng, M. Feng, H. Han, J. Wang, *J. Phys. Chem. Lett.* **2017**, 8, 1804.
- [27] W. Chen, J. Hao, W. Hu, Z. Zang, X. Tang, L. Fang, T. Niu, M. Zhou, *Small* **2017**, 13, 1604085.
- [28] G. Yang, Q. Fan, B. Chen, Q. Zhou, H. Zhong, *J. Mater. Chem. C* **2016**, 4, 11387.
- [29] S. N. Raja, Y. Bekenstein, M. A. Koc, S. Fischer, D. Zhang, L. Lin, R. O. Ritchie, P. Yang, A. P. Alivisatos, *ACS Appl. Mater. Interfaces* **2016**, 8, 35523.
- [30] Z. J. Li, E. Hofman, J. Li, A. H. Davis, C. H. Tung, L. Z. Wu, W. Zheng, *Adv. Funct. Mater.* **2018**, 28, 1704288.
- [31] C. Sun, Y. Zhang, C. Ruan, C. Yin, X. Wang, Y. Wang, W. Yu, *Adv. Mater.* **2016**, 28, 10088.
- [32] Z. Li, L. Kong, S. Huang, L. Li, *Angew. Chem., Int. Ed.* **2017**, 56, 8134.
- [33] H. C. Wang, S. Y. Lin, A. C. Tang, B. P. Singh, H. C. Tong, C. Y. Chen, Y. C. Lee, T. L. Tsai, R. S. Liu, *Angew. Chem., Int. Ed.* **2016**, 55, 7924.
- [34] S. Huang, Z. Li, L. Kong, N. Zhu, A. Shan, L. Li, *J. Am. Chem. Soc.* **2016**, 138, 5749.
- [35] Z. Hu, Z. Liu, Y. Bian, S. Li, X. Tang, J. Du, Z. Zang, M. Zhou, W. Hu, Y. Tian, Y. Leng, *Adv. Opt. Mater.* **2018**, 6, 1700997.
- [36] A. H. Lu, E. L. Salabas, F. Schuth, *Angew. Chem., Int. Ed.* **2007**, 46, 1222.
- [37] A. L. Rogach, D. Nagesha, J. W. Ostrander, M. Giersig, N. A. Kotov, *Chem. Mater.* **2000**, 12, 2676.
- [38] M. Lal, L. Levy, K. S. Kim, G. S. He, X. Wang, Y. H. Min, S. Pakatchi, P. N. Prasad, *Chem. Mater.* **2000**, 12, 2632.
- [39] A. P. Philipse, M. P. B. Bruggen, C. Pathmanoharan, *Langmuir* **1994**, 10, 92.
- [40] C. Hui, C. Shen, J. Tian, L. Bao, H. Ding, C. Li, Y. Tian, X. Shi, H. J. Gao, *Nanoscale* **2011**, 3, 701.
- [41] S. H. Joo, J. Y. Park, C. K. Tsung, Y. Yamada, P. Yang, G. A. Somorjai, *Nat. Mater.* **2009**, 8, 126.
- [42] H. Huang, F. Zhao, L. Liu, F. Zhang, X. Wu, L. Shi, B. Zou, Q. Pei, H. Zhong, *ACS Appl. Mater. Interfaces* **2015**, 7, 28128.
- [43] S. T. Selvan, T. T. Tan, *Adv. Mater.* **2005**, 17, 1620.
- [44] Z.-J. Li, E. Hofman, A. H. Davis, M. M. Maye, W. Zheng, *Chem. Mater.* **2018**, 30, 3854.
- [45] L. Xu, J. Chen, J. Song, J. Li, J. Xue, Y. Dong, B. Cai, Q. Shan, B. Han, H. Zeng, *ACS Appl. Mater. Interfaces* **2017**, 9, 26556.
- [46] M. Michalska, A. Aboulaich, G. Medjahdi, R. Mahiou, S. Jurga, R. Schneider, *J. Alloys Compd.* **2015**, 645, 184.
- [47] Y. Shirasaki, G. J. Supran, M. G. Bawendi, V. Bulović, *Nat. Photonics* **2013**, 7, 13.
- [48] Q. A. Akkerman, V. D'Innocenzo, S. Accornero, A. Scarpellini, A. Petrozza, M. Prato, L. Manna, *J. Am. Chem. Soc.* **2015**, 137, 10276.
- [49] C. C. Lin, A. Meijerink, R.-S. Liu, *J. Phys. Chem. Lett.* **2016**, 7, 495.
- [50] Z. Li, L. Kong, S. Huang, L. Li, *Angew. Chem.* **2017**, 129, 8246.
- [51] H.-C. Wang, S.-Y. Lin, A.-C. Tang, B. P. Singh, H.-C. Tong, C.-Y. Chen, Y.-C. Lee, T.-L. Tsai, R.-S. Liu, *Angew. Chem.* **2016**, 128, 8056.
- [52] W. Chen, T. Shi, J. Du, Z. Zang, Z. Yao, M. Li, K. Sun, W. Hu, Y. Leng, X. Tang, *ACS Appl. Mater. Interfaces* **2018**, 10, 43978.
- [53] F. Fang, W. Chen, Y. Li, H. Liu, M. Mei, R. Zhang, J. Hao, M. Mikita, W. Cao, R. Pan, K. Wang, X. W. Sun, *Adv. Funct. Mater.* **2018**, 28, 1706000.
- [54] S. Sun, D. Yuan, Y. Xu, A. Wang, Z. Deng, *ACS Nano* **2016**, 10, 3648.
- [55] X. Zhang, X. Bai, H. Wu, X. Zhang, C. Sun, Y. Zhang, W. Zhang, W. Zheng, W. W. Yu, A. L. Rogach, *Angew. Chem., Int. Ed.* **2018**, 57, 3337.
- [56] M. Liu, G. Zhong, Y. Yin, J. Miao, K. Li, C. Wang, X. Xu, C. Shen, H. Meng, *Adv. Sci.* **2017**, 4, 1700335.
- [57] F. Zhang, H. Zhong, C. Chen, X. Wu, X. Hu, H. Huang, J. Han, B. Zou, Y. Dong, *ACS Nano* **2015**, 9, 4533.